






## Seismic facies characterization using Rock Physics Templates and brittleness indices: Stybarrow field

Daniel López-Aguirre<sup>1</sup>, Miguel Ángel Domínguez-Cruz<sup>1</sup>, José Aurelio España-Pinto<sup>2</sup>, Oscar Cerapio Valdiviezo-Mijangos<sup>2</sup> and Rubén Nicolás-López<sup>3</sup>.

### Abstract

This paper proposes a method for identifying the lithological properties of the medium based on the joint analysis of the Lamé parameters, Young's Modulus, and Poisson's Ratio. Additionally, an analysis of brittleness was proposed to identify brittle/ductile intervals and areas of potential reservoirs. The petroelastic properties were analyzed at well and seismic scales using ternary rock physics templates. These templates were built from a self-consistent micromechanical model. In addition, the analysis allows for preserving the conditions of the environment subsurface in the seismic and log information. A workflow for petroelastic lithology interpretation was coupled with a workflow of brittleness modeling. The results correlate well with conventional qualitative methodologies applied in previous studies. A brittleness analysis methodology was developed and tested to identify reservoirs associated with the Lower Cretaceous in the Stybarrow field in Australia; the results highlight the high brittleness zones attenuated by hydrocarbons ( $BA \geq 0.5$ ). The proposed seismic-based methodology is an improvement to conventional analysis trends for identifying lithologies and prospective hydrocarbon zones.

**Key words:** Elastic modulus, Petroelastic model, Brittleness, Rock Physics Templates.

### Resumen

Se propone un método para identificar las propiedades litológicas del medio basado en el análisis conjunto de los parámetros de Lamé, Módulo de Young y Relación de Poisson. También se propone un análisis de fragilidad para identificar intervalos frágiles/dúctiles y áreas potenciales de yacimientos. Las propiedades petroelásticas se analizaron a escala sísmica y de pozo utilizando plantillas ternarias de física de rocas. Las plantillas ternarias se construyeron con un modelo micromecánico auto-consistente. El análisis permite preservar las condiciones del ambiente del subsuelo en la información sísmica y de registros. Se combinó un flujo de trabajo para la interpretación petroelástica de litologías con un flujo de trabajo de modelado de la fragilidad. Los resultados se correlacionan bien con las metodologías cualitativas convencionales aplicadas en estudios previos. Además desarrolló y probó una metodología de análisis de fragilidad para identificar yacimientos asociados con el Cretácico Inferior en el campo Stybarrow en Australia; los resultados resaltan las zonas de alta fragilidad atenuadas por hidrocarburos ( $BA \geq 0.5$ ). La metodología propuesta basada en sísmica es una mejora a las tendencias de análisis convencionales para identificar litologías y zonas prospectivas de hidrocarburos.

**Palabras clave:** módulos elásticos, modelo petroelástico, fragilidad, plantillas de física de rocas.

Received: June 19, 2023; Accepted: November 7, 2023; Published on-line: January 1, 2024.

Editorial responsibility: Dra. Alexandra Ossa López

\* Corresponding author: Rubén Nicolás-López, [rnlopez@imp.mx](mailto:rnlopez@imp.mx)

<sup>1</sup> Instituto Mexicano del Petróleo, Dirección de Desarrollo de Talento, Posgrado IMP, Ciudad de México, México. CP 07730

<sup>2</sup> Instituto Mexicano del Petróleo, Dirección de Servicios en Exploración y Producción, Ciudad de México, México. CP 07730

<sup>3</sup> Instituto Mexicano del Petróleo, Dirección de Tecnología de Producto, Ciudad de México, México. CP 07730

Daniel López-Aguirre, Miguel Angel Domínguez-Cruz, José Aurelio España-Pinto, Oscar Cerapio Valdiviezo-Mijangos, Rubén Nicolás-López.

<https://doi.org/10.22201/igeof.2954436xe.2024.63.1.1716>

## 1. Introduction

Rock characterization based on elastic responses that consider mineralogical composition and pore-filling fluids at the core, well, and field scales have been reported by rich literature on rock physics applied to earth models (Goodway and Pérez 2010, Meléndez and Schmitt 2013, Perez and Mafurt 2014, Nicolás-López and Valdiviezo-Mijangos 2016, Carcione and Avseth, 2015, Sayar and Torres-Verdín 2017, Holt and Westwood, 2016, Nicolás-López *et al.*, 2019, and Nicolás-López *et al.*, 2020). However, most of these reported applications are related to petroelastic models constructed from classical static Gassmann models or dynamic micromechanical models for lithology interpretation and reservoir delineation.

The petroelastic models can be defined as a connection between reservoir properties and seismic attributes of the subsurface structures. This connection is used to link seismic parameters such as acoustic and shear impedances ( $I_p$  &  $I_s$ )

with rock's elastic parameters as shear modulus ( $\mu$ ), Lamé parameter ( $\lambda$ ), Young's Modulus ( $E$ ), and Poisson's ratio ( $\nu$ ) (Danaei *et al.*, 2020). A well-known methodology for interpreting the amplitudes from pre-stacked seismic reflection data to produce a probabilistic distribution of subsurface lithology and pore fluid information is described in Avseth *et al.* (2005). As part of this sort of contribution, in which relationships between seismic and elastic parameters are noted, the job of Danaei *et al.* (2020) has established a connection between petroelastic information and 4D seismic information. It was carried out to optimize volumes to identify pore pressure and fluid saturation variations. Similarly, Uhlemann *et al.* (2016) correlated the seismic velocities with seismic tomography to highlight the importance of the modulus of elasticity ( $M$ ) for a better characterization in identifying potential hydrocarbon zones with seismic images of high resolution. Bredesen *et al.* (2021) demonstrated how to perform a quantitative reservoir characterization using rock physics models on

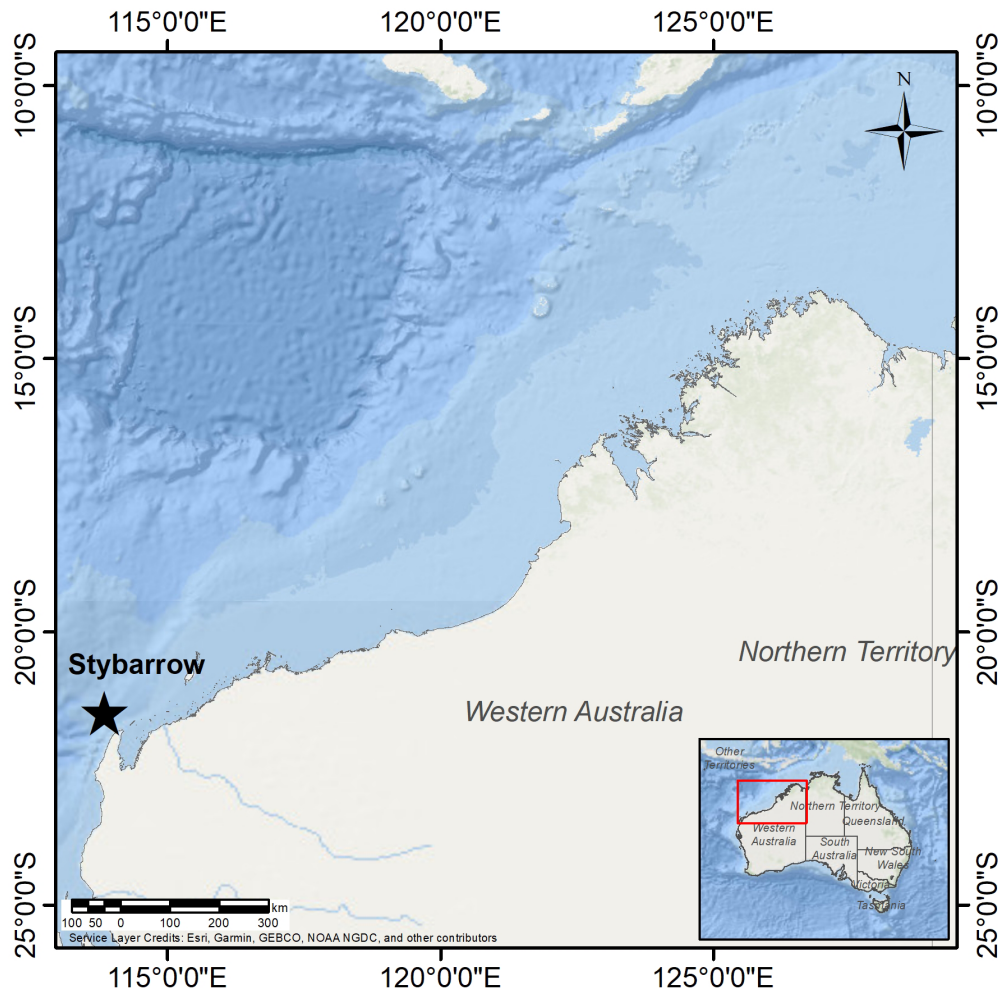


**Figure 1.** The geographic location of the study area.

Source: Generated from Gavin (2015).

seismic inversion data, achieving consistent predictions of a gas-condensate reservoir.

In the present study, we also worked with rock's elastic parameters, e.g., the modulus of elasticity, lambda-rho, or mu-rho, with the difference that a micromechanical quantitative method was used. This investigation focused on identifying potential prospective hydrocarbon reservoir zones through the lithological interpretation workflow via computing elastic properties from well-logs and seismic volumes. The objective was to establish the coupled relationship that exists between the elastic parameters at well and seismic scales to determine the lithological configuration of a study area, thus simplifying the scaling process and the prediction and identification of lithologies and areas of oil interest (reservoir) making possible the scaling of any elastic parameter in 3D seismic inversion data.

The novel methodology using a micromechanical model proposed here makes it possible to identify lithologies and prospective hydrocarbon zones. It also includes a new feature: 1D-3D brittleness workflows for identifying the reservoir zones. Both petroelastic and brittleness workflows were applied to identify a reservoir in the Lower Cretaceous associated with the Stybarrow field through quantitative (hard) results ( $BA \geq 0.5$ ). The results were consistent with those reported using other methodologies (Ementon *et al.*, 2004; Arevalo-López 2017). Therefore, the proposed methodology represents an alternative to identifying potential oil or gas zones.

### 1.1. Geology setting: Barrow subbasin

The field information consists of geophysical logs and seismic information from a study area in deep water to the NW of Australia known as the Carnarvon Basin (Figure 1), which is a marine oil and gas-producing basin containing up to 10 km thicknesses of predominantly Mesozoic deltaic siliciclastics (Ementon *et al.*, 2004).

The Barrow Sub-basin is geologically an elongated marine basin trending NNE to SSW, which forms part of the North Carnarvon Basin in Northwest Australia. The Barrow Sub-basin is a deep syncline graben that forms a depocentre of about 10 km of predominantly Mesozoic and Cenozoic sequences, which are flanked to the east and west by shallow faulted terraces containing more than 5 km of Paleozoic strata from Cenozoic (Ementon *et al.*, 2004).

The development of the basin began in the Paleozoic, generating structural changes due to intense opening processes during the Late Triassic to Early Jurassic that occurred between Australia and the Burma Block to the West of India. During the Late Triassic to Early Jurassic, deltaic sand reservoirs of fluvial and coastal origin occurred. Later a transgressive phase of ma-

rine clastic sedimentation occurred in the Early to Late Jurassic. Subsequent extension events occurred during the Middle-Late Jurassic and Early Cretaceous. In contrast, for the Late Cretaceous, an inversion process led to compression until the Miocene, creating several structural traps within the Barrow Sub-basin. As a result, the Barrow Delta was prograded northward through the Barrow Sub-basin during the Early Cretaceous. It was followed by a transgressive phase of marine clastic sedimentation until the Middle Cretaceous (Ementon *et al.*, 2004).

The main exploration plays in the Barrow Sub-basin comprise anticlines and fault-limited structures, with the regional seal formed by Early Cretaceous deep marine shales. The accumulations of hydrocarbons are found predominantly in the Lower Cretaceous in siliciclastic rocks of continental origin of the volcanic type; due to this, in the storage rock of the study reservoir, we find the presence of sandstones with the content of Potassium Feldspars as well as a variety of clays among the main ones: kaolinite, smectite, and illite. Most oil and gas accumulations come from Upper Jurassic marine shales (source rock). The main pulse of hydrocarbon generation in the Upper Jurassic source rocks occurred during the Early Cretaceous and continued throughout the Late Cretaceous to the Cenozoic.

### 1.2. Case study: Stybarrow field

To deploy a field application of the proposed methodology, we used available stacked seismic information of the Stybarrow deepwater field, as well as the information of four wells (Stybarrow-1, Stybarrow-2, Stybarrow-3, and Stybarrow-4), from which the geological formations overlying and underlying the Lower Cretaceous reservoir were selected. The measured depths of wells range from the sea level to 2,100 m and 2,400 m approximately (Figure 2).

#### 1.2.1. Lithology units

A selection of homologated stratigraphic peaks determined from qualitative analysis of the gamma-ray log was made for the four wells used in the proposed methodology (Figure 2). It derived from the little homogeneity in the information available. The available well logs of the Stybarrow-1, Stybarrow-2, Stybarrow-3, and Stybarrow-4 wells in the study area with which the proposed methodology are shown in Table 1.

In Figure 2, the GR log of the four wells in the Stybarrow field is displayed according to their geographic position from SW to NE, Stybarrow-2 (Sty-2), Stybarrow-1 (Sty-1), Stybarrow-4 (Sty-4), and Stybarrow-3 (Sty-3). Also, the reservoir zones penetrated by each well were highlighted with orange shading, highlighting that the Sty-3 no longer cut the reservoir, becoming a delimiting well of the field. As the Sty-1 well has

**Table 1.** Geophysical logs were available for the wells in the study area. These logs are essential to construct a petroelastic model.

Well Log	Sty-1	Sty-2	Sty-3	Sty-4
Interval [m]	1,906-2,460	1,800-2,350	1,960-2,500	1,955-2,485
GR	♦	♦	♦	♦
RHOB	♦	♦	♦	♦
Vp	♦	♦	♦	♦
Vs	♦		♦	

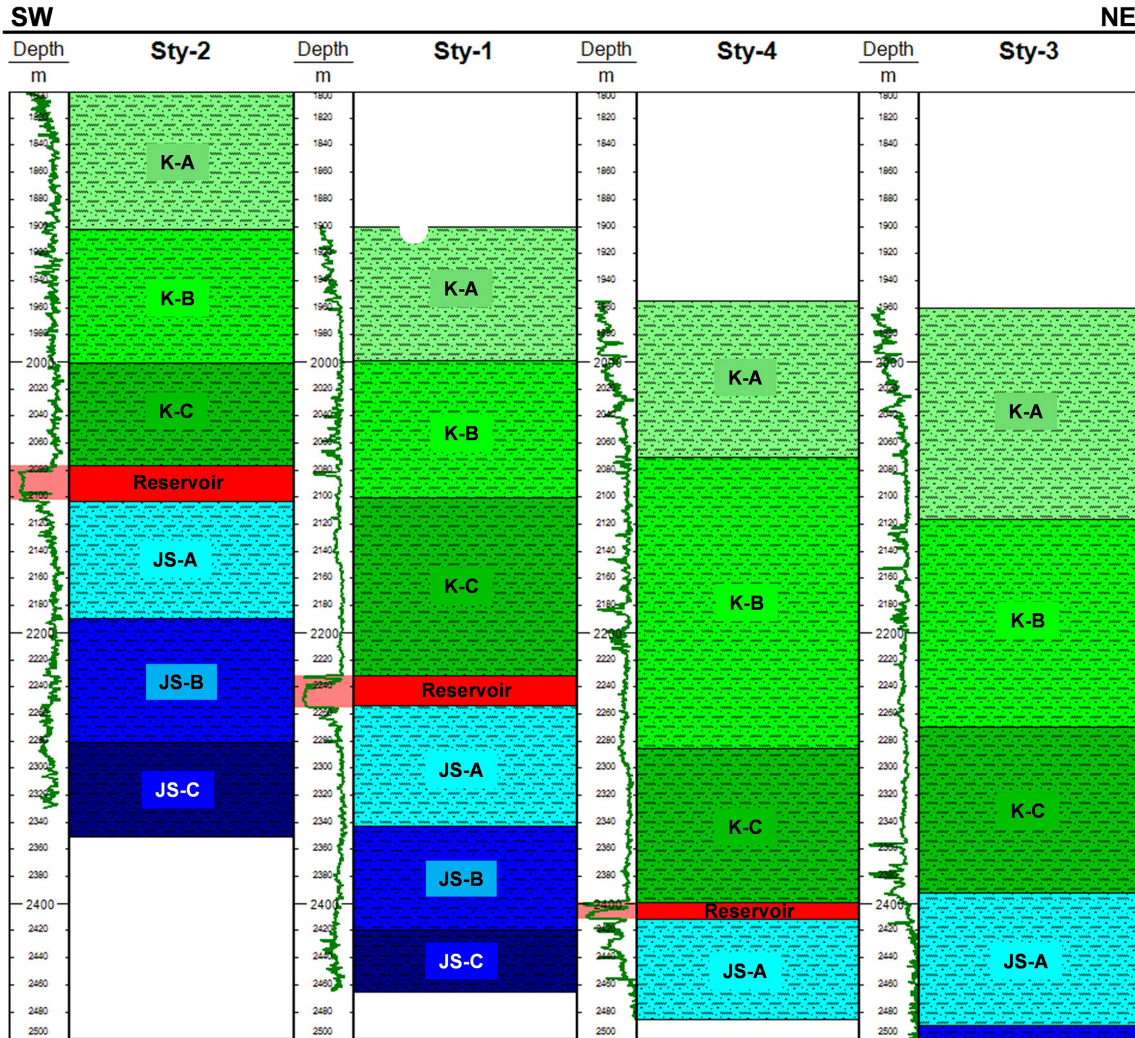


**Figure 2.** The correlation of the wells in the study area, represented from left to right, is the Gamma Ray (GR) log of the Stybarrow-2, Stybarrow-1, Stybarrow-4, and Stybarrow-3 wells.

complete information, it was from the results obtained for this well that the results for the other wells and seismic data of the area were calibrated.

**1.2.2. Well and seismic inversion data**

Herein, we used well data and volumes of inverted elastic

parameters provided by Stanford University. The detailed process of seismic inversion modeling is described in Arévalo-López (2017). The inversion process by which the volumes of  $I_p$ ,  $I_s$ , and  $RHOB$  were obtained is called simultaneous impedance inversion, performed using a constrained sparse-spike inversion algorithm based on the optimization of the L1 norm. This algorithm creates an ensemble of elastic models using

multiple partial angle stacks of seismic data (Areválo-López and Dvorkin, 2017).

A set of elastic models using multiple seismic partial angle stacks were generated in Areválo-López (2017). To achieve this, Aki-Richards equations were used to compute the reflection coefficients at seismic scale, while at well scale (low frequency), P and S velocities are used for the elastic model. Inversion process usually includes QC on input data, cross correlation between the angle stacks for obtaining time-aligned stacks, seismic-to-well tie, wavelet extraction for each angle gathers, horizon interpretation based on the near-stack amplitude, well- and horizon-based low frequency models of  $I_p$ ,  $I_s$ , and density of the earth model, inversion parameter optimization, and quality control of the inversion results.

Inversion parameters were optimized to obtain the best fit between the seismically derived values and the data from Well Sty-1. Subsequently, these parameters were used to obtain the simultaneous impedance inversion for the entire seismic cube. The most critical optimization parameter was the "contrast mismatch" that controls the variance of the elastic parameters between the inversion results and the low-frequency well data (Figure 3).

According to Arévalo-López (2017), the key to obtaining an acceptable seismic inversion is to match the seismically derived Poisson's ratio with the same parameter calculated from well-log data.

## 2. Petroelastic and Brittleness workflows

### 2.1. Petroelastic model

This study extended the 1D methodology to implement self-consistent models SCM proposed by Nicolás-López and Valdiviezo-Mijangos (2016) to a 3D petroelastic workflow for

lithotype interpretation. SCM was applied to obtain rock's elastic effective properties considering a heterogeneous medium of inclusions (minerals, fluids, or organic matter) for different porosity scenarios. The self-consistent method equations introduced by Sabina and Willis (1988) are non-linear; Valdiviezo-Mijangos and Nicolás-López (2014) solved them with the fixed-point method. When obtaining the solution of the equations, it is assumed that the properties of the rock  $\mu$ ,  $\kappa$  and  $\rho$  of a homogeneous system become properties of a heterogeneous system, which are called effective properties ( $\mu_0$ ,  $\kappa_0$  y  $\rho_0$ ).

Self-consistent equations for  $n$  inclusions are,

$$\kappa_0 = \kappa_{n+1} + \sum_{r=1}^n \frac{\alpha_r (\kappa_r - \kappa_{n+1})}{1 + 3(\kappa_r - \kappa_0) / (3\kappa_0 + 4\mu_0)} \quad (1)$$

$$\mu_0 = \mu_{n+1} + \sum_{r=1}^n \frac{\alpha_r (\mu_r - \mu_{n+1})}{1 + 6(\mu_r - \mu_0) [(\kappa_0 + 2\mu_0)] / [5\mu_0 (3\kappa_0 + 4\mu_0)]} \quad (2)$$

$$\rho_0 = \rho_{n+1} + \sum_{r=1}^n \alpha_r (\rho_{r+1}) \quad (3)$$

where  $\kappa_0$  is the effective bulk modulus,  $\kappa_{n+1}$  is the bulk modulus of the matrix,  $\kappa_r$  is the bulk modulus of an inclusion,  $\alpha_r$  is the volume fraction of inclusions,  $\mu_0$  is the effective shear modulus,  $\mu_{n+1}$  is the shear modulus of the matrix,  $\mu_r$  is the shear modulus of inclusion,  $\rho_0$  is the effective bulk density,  $\rho_{n+1}$  is the density of matrix, and  $\rho_r$  is the inclusion density.

The self-consistent equations, (1) to (3), were used to construct the rock physics templates RPT in terms of Mu-Rho ( $\mu\rho$ ) vs. Lambda-Rho ( $\lambda\rho$ ) where  $\lambda = \kappa_0 + \frac{2}{3}\mu_0$ . These equations consider elastic contributions of rock constituents based on mineral content and pore-filling fluids.

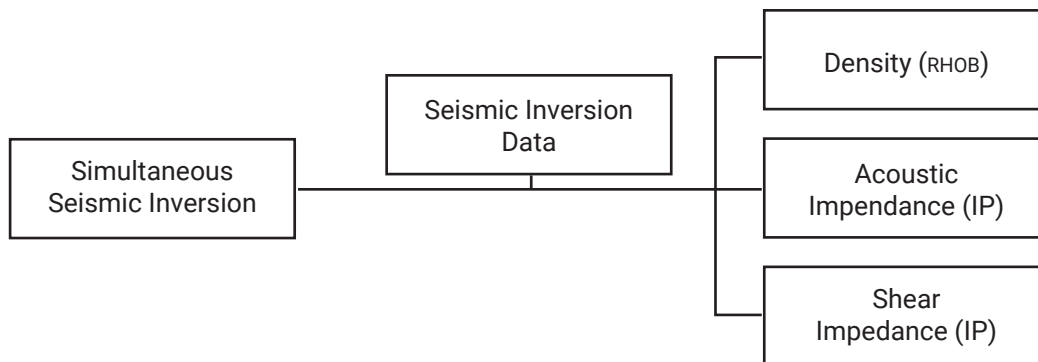


**Figure 3.** The sequence used to obtain volumes of elastic properties through simultaneous Seismic Inversion (Arévalo-López, 2017).

## 2.2. Brittleness models

This work proposed the integrated analysis of lithology's petroelastic interpretation and brittleness evaluation. Elastic parameters  $\mu\rho$  and  $\lambda\rho$  are convenient for construing 1D-3D lithology models, and  $E$  and  $\nu$  are for qualitative brittleness evaluation. The brittleness models defined by Rickman *et al.* (2008) and worked by Lizcano *et al.* (2018) considered the use of rock physics templates to define pay zones guided by mineral fractions of a lithology column. They were used to construct a novel 1D-3D brittleness and petroelastic workflow.

### Brittleness index based on Young's modulus ( $BI_E$ )

This brittleness index is defined by normalization of Young's modulus, taking as its limits the maximum and minimum values of a sedimentary column. In an  $(E - \nu)$  cross-plot, the results usually generate horizontal straight lines because  $E$  only varies.  $BI_E$  is calculated with the following equation,

$$BI_E = \frac{E - E_{min}}{E_{max} - E_{min}} \quad (6)$$

where  $E$  is Young's modulus,  $E_{min}$  is the minimum Young's modulus, and  $E_{max}$  is the maximum Young's modulus. For practical applications, higher values of Young's modulus are related to brittle formations and lower to ductile formations.

### Brittleness index based on Poisson's ratio ( $BI_\nu$ )

The normalization considers Poisson's ratio from a sedimentary column's maximum and minimum values. Poisson's ratio always has values between 0 and 0.5. This parameter generates vertical straight lines when superimposed on  $(E - \nu)$  cross-plot. It is computed with the following equation,

$$BI_\nu = \frac{\nu - \nu_{max}}{\nu_{min} - \nu_{max}}, \quad (7)$$

where  $\nu$  is Poisson's ratio,  $\nu_{min}$  is the minimum Poisson's ratio, and  $\nu_{max}$  is the maximum Poisson's ratio. Higher values of Poisson's ratio are always linked to ductile formations and lower to brittle formations.

### Average Brittleness index ( $BA$ )

As for heuristics,  $BI_E$  and  $BI_\nu$  must be considered to improve brittleness evaluation. Therefore,  $BA$  is determined via the li-

near average between the values of  $BI_E$  and  $BI_\nu$ . This parameter generates oblique straight lines when they are superimposed on  $(E - \nu)$  cross-plot and with which can be performed brittleness analysis. The average brittleness index is obtained with the following expression,

$$BA = \frac{BI_\nu + BI_E}{2} \quad (8)$$

where  $BI_E$  and  $BI_\nu$  were defined in equations (6) and (7).

## 2.3. Workflow for 1D-3D lithotype interpretation

The proposed workflow for 1D-3D lithotype interpretation is based on rock physics templates RPT which have risen as efficient tools for lithotype interpretation (Nicolas-López *et al.*, 2019). They were constructed similarly described in Nicolás-López and Valdiviezo-Mijangos (2016). Therefore, a new workflow for 3D lithotype interpretation was set up. The lithologies were identified from their 1D-3D elastic properties computed at well and field scale. It is worth mentioning that the same calibrated  $(\mu\rho - \lambda\rho)$  RPT was used for  $\mu\rho$  and  $\lambda\rho$  calculated with geophysical logs and seismic inversion data.

In Figure 4, the steps for 1D-3D lithotype interpretation are shown. First, the geometry and consistency of data clouds of petroelastic parameters and density were validated for well and field scales. Next, supervised quality control must be conducted for seismic inversion data and well logs. Finally, the missed data were correlated, honoring the lithology reported in analog wells. Next,  $(\mu\rho - \lambda\rho)$  RPT based on three dominant minerals was developed using the self-consistent equations, Eqs. (1) to (3). Elastic properties of pure dominant minerals define the vertexes of RPT; for instance: quartz, feldspar, and clay are often dominant minerals for terrigenous formations, and clay, calcite, and dolomite for carbonate formations. After RPT designing, lithotype interpretation is conducted using lithological zones related to lithotypes' elastic properties. Finally, the 1D-3D interpretation results are lithotype logs for wells analyzed and the volume of lithotypes.

## 2.4. Workflow for 1D-3D brittleness analysis

For well and field scale, lithology interpretation was suggested by calibrated  $(\mu\rho - \lambda\rho)$  RPT. Nevertheless, we have proposed novel integrated workflows to couple brittleness analysis with petroelastic lithotype interpretation to enhance robustness, Figure 5. Reservoir delineation is improved because defining higher-brittleness zones aims to plan optimized well surveys for better hydrocarbon exploitation. First, the brittleness analysis is proposed using lithology-based limits to Young's modulus  $E$

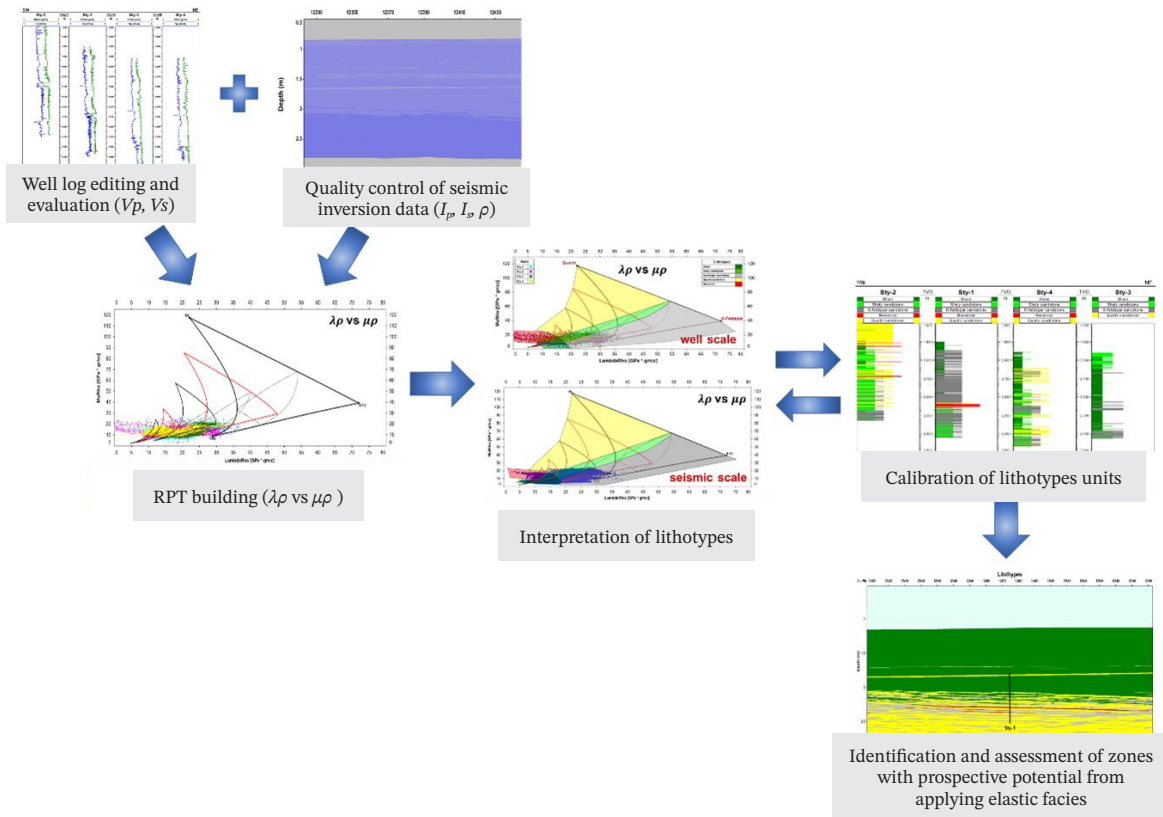


**Figure 4.** Workflow for 1D-3D lithotype interpretation using ternary rock physics templates. Petroelastic analysis sequence to relate seismic with well logs for obtaining lithotype logs and volume of lithotypes. Ternary rock physics templates were generated considering the 1D methodology described in Nicolás-López and Valdiviezo-Mijangos (2016).

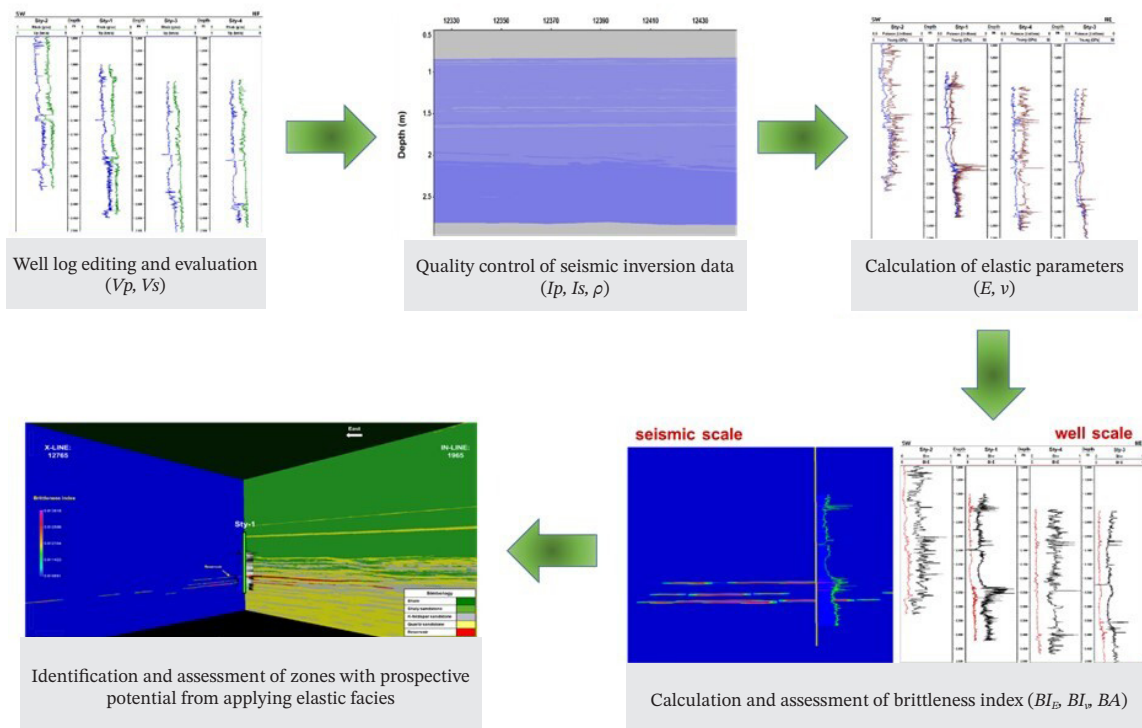


**Figure 5.** Novel workflow for 1D-3D brittleness analysis for identifying areas with reservoir potential using enhanced 1D brittleness methodology (Lizcano et al., 2018).

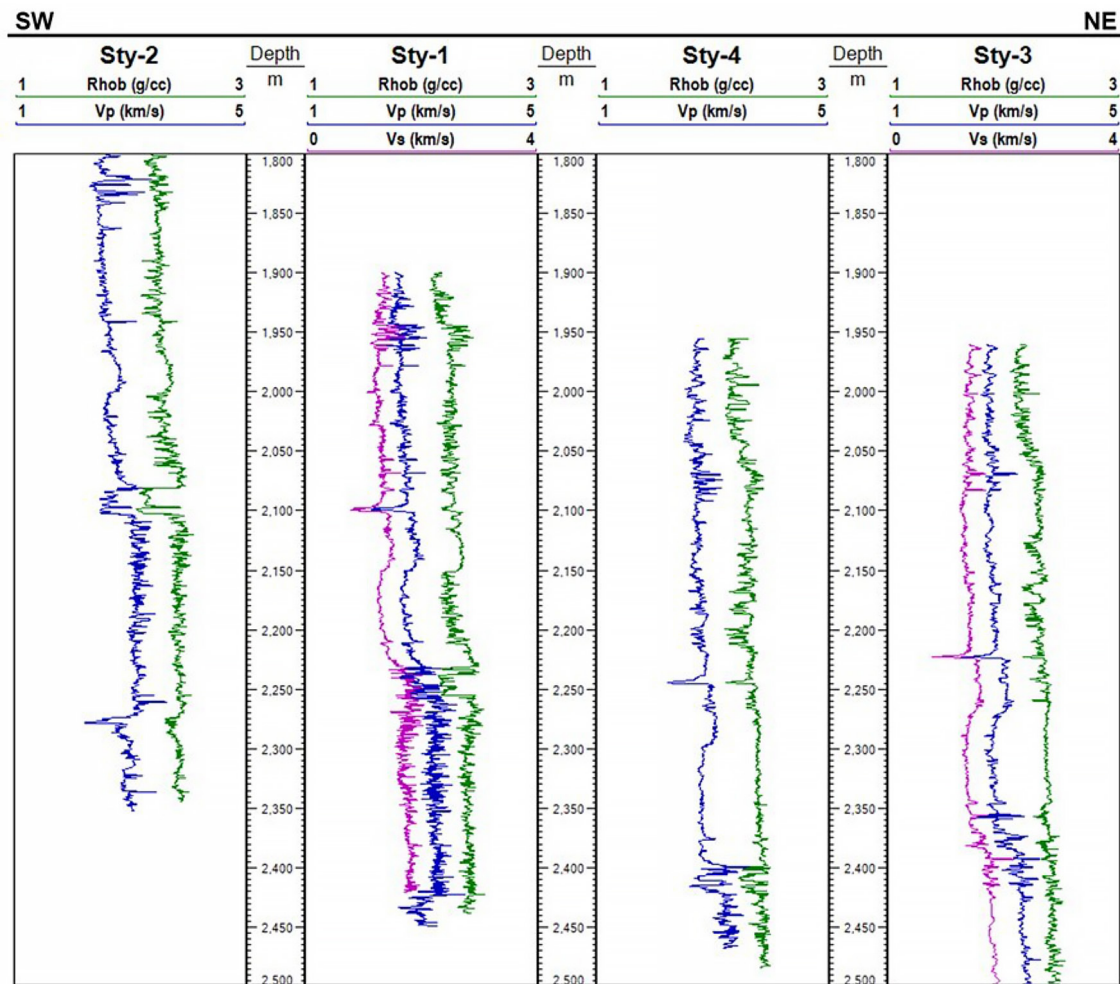


**Figure 6.** Logs of density and elastic parameters,  $V_p$  and  $V_s$  are shown. Wave velocities were calculated from transit time logs. Shear wave velocity  $V_s$  was solely available in Sty-1 and Sty-3.

and Poisson's ratio  $\nu$ . The  $E$  maximum and minimum used are related to brittle rocks. Conversely,  $E$  minimum and  $\nu$  maximum are related to ductile rocks; next, brittleness indexes in Eqs. (6) to (8) are calculated using geophysical well logs and volumes of elastic moduli. Next, cut-off values evaluate Brittleness logs and brittleness volumes to define reservoir zones prone to hydraulic stimulation. Finally, the petroelastic interpretation and brittleness analysis results are correlated to characterize zones for well placement.

### 3. Results

#### 3.1. Characterization of density and rock's elastic properties

1D-3D petroelastic interpretation and brittleness workflows require a rigorous characterization of density and rock's elastic properties. The required curves to determine elastic properties

that will be scaled to seismic information were mainly wet bulk density  $RHOB$ , compressional  $V_p$ , and shear  $V_s$  wave velocities. In this case study, they were available for the Sty-1 and Sty-3 wells (Figure 6). In Sty-2 and Sty-4 wells, it is solely accounted with  $RHOB$  and  $V_p$ .

Therefore, it was necessary to compute  $V_s$  data for all wells involved in the novel petroelastic modeling proposed. To obtain  $V_s$  values with an acceptable accuracy to Sty-2 and Sty-4 wells, a neural networks NN methodology like the one proposed by López-Aguirre *et al.* (2020) was followed. Herein,  $V_s$  curves of Sty-1 and Sty-3 wells with a vertical resolution of 0.1524 m were used as data in training mode; while the wells that did not have  $V_s$  were included with a lower vertical resolution (2 m) in the data set defined like test mode. After the NN process was executed,  $V_s$  curves for Sty-1 and Sty-3 were modeled (Figure 7). Then, the analysis results for the training wells were compared with the hard data with which a high correlation was obtained. Finally,  $V_s$  curves were obtained for the wells that did not have them.



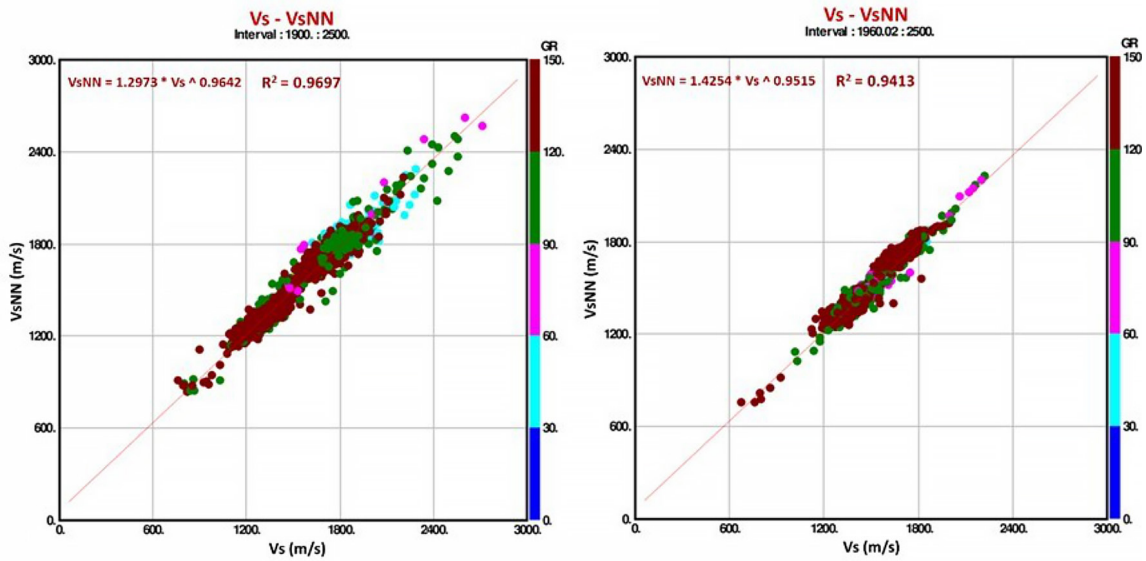


**Figure 7.** Analysis of the  $V_s$  results obtained from neural networks NN. The left figure shows  $V_s$  results obtained for the Sty-1, while the right figure shows the results of  $V_s$  for the Sty-3 well.

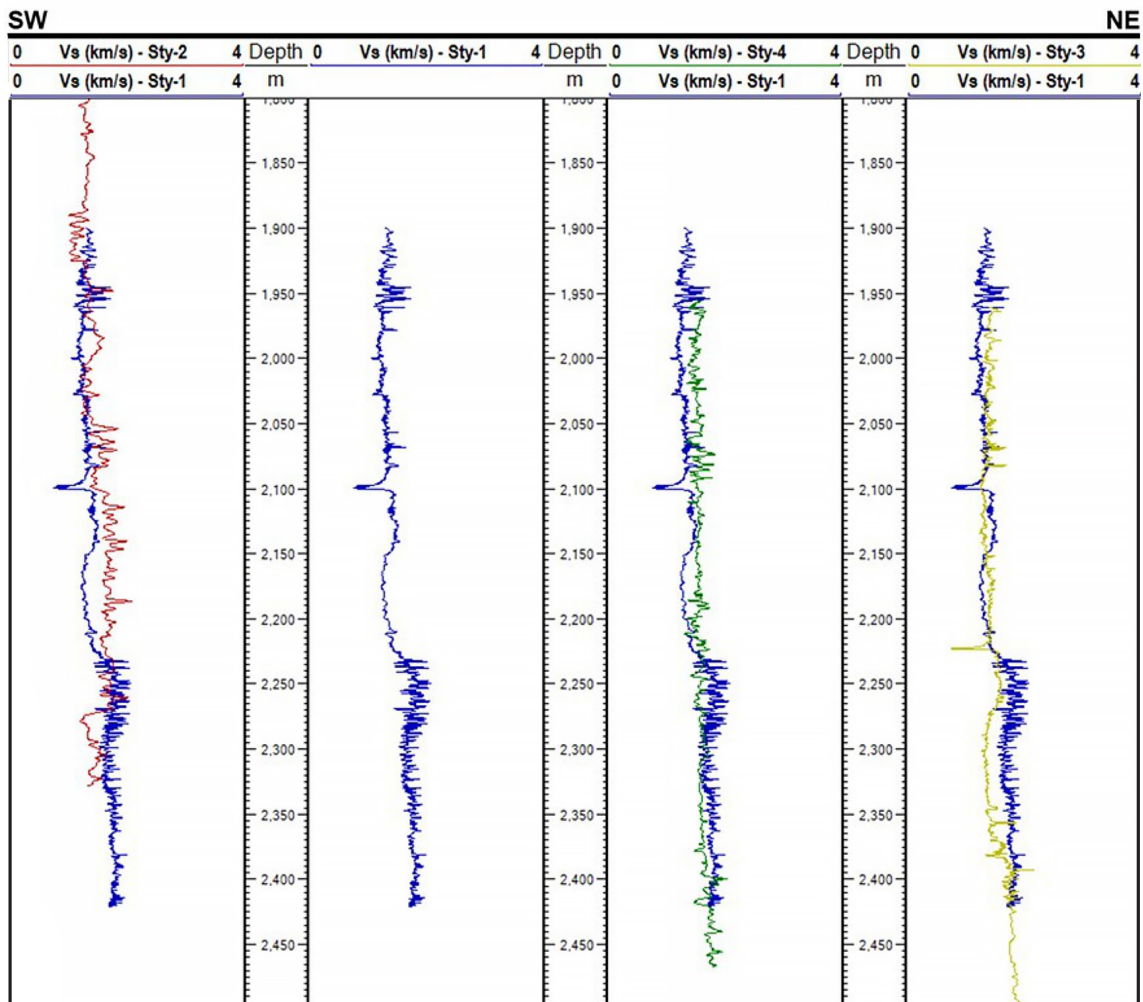


**Figure 8.** Value-range-based calibration of modeled  $V_s$  well logs. Sty-1 is the correlation well for qualitative analysis in tracks.

Figure 8 shows the validation of  $V_s$  results obtained with NN against actual  $V_s$  logs for the Sty-1 and Sty-3 wells. The relationships obtained are those mentioned in the following equations,

$$V_{s_{NN}} = 1.29V_s^{0.96} \text{ for Sty-1,} \tag{9}$$

$$V_{s_{NN}} = 1.42V_s^{0.95} \text{ for Sty-3.} \tag{10}$$

Next,  $V_s$  logs calculated with NN for Sty-2 and Sty-4 wells also have equivalent accuracy of around 95%. In addition, the value range of the four  $V_s$  curves estimated with NN is qualitatively placed in context using Sty-1  $V_s$  log, Figure 8. After these realizations of  $V_s$ , we have completed the set of density  $RHO_B$ , compressional  $V_p$ , and shear  $V_s$  wave velocity for petroelastic interpretation of lithology columns.

### 3.2. Petroelastic parameters

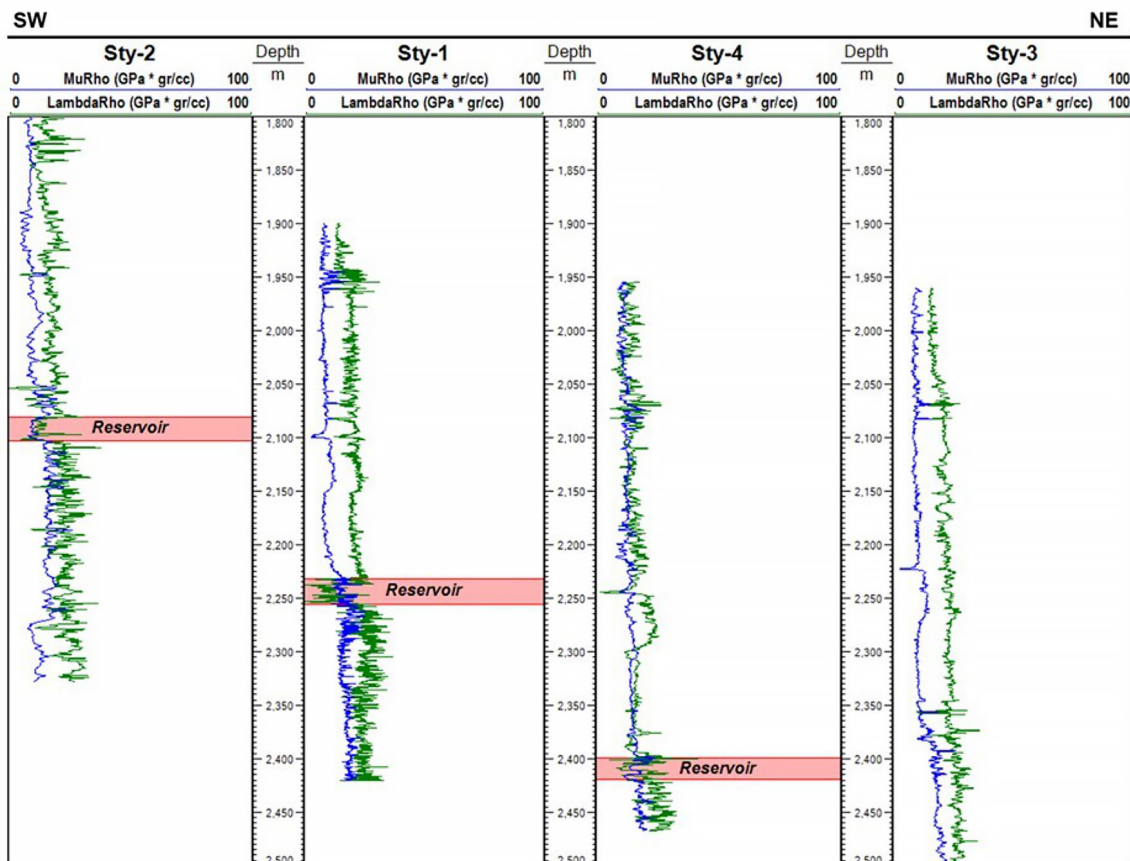
The elastic parameters Mu-Rho ( $\mu\rho$ ) and Lambda-Rho ( $\lambda\rho$ ) to each well of the study case were calculated using well logs called bulk density  $RHO_B$ , compressional  $V_p$ , and shear  $V_s$  wave velocity,

Figure 9. They are central inputs to petroelastic interpretation workflows of lithologies and the presence of pore fluids. Note that Mu and Lambda are non-dependent elastic parameters, and both are impacted with bulk density to highlight the presence of pore-filling fluids. On the other hand,  $\mu\rho$  is always less than  $\lambda\rho$  because it is only sensitive to rock matrix, leaving out the pore fluids effect.

### 3.3. 1D petroelastic model for lithotype interpretation

RPT-based interpretation of lithotypes usually starts with defining lithology classification from the field description reported (Nicolás *et al.*, 2019). From the geological information of the study area, the lithologies are linked to dominant minerals, i.e., shale is related to clay minerals, and sandstone to quartz. Sandstones can also be discriminated via the content of the second dominant mineral, Table 2. Therefore, the column was primarily defined by lithologies considering mineralogy content.

After defining the lithologies that constitute the lithology column, the elastic properties of three dominant minerals were determined to build the specific RPT for the study area. First, we



**Figure 9.** The elastic parameters, Mu-Rho ( $\mu\rho$ ) and Lambda-Rho ( $\lambda\rho$ ) in GPa, were obtained for the wells of the study case. Reservoir intervals reported in wells from Figure 2.

defined two siliciclastic minerals (quartz and potassium feldspar) and one argillaceous mineral (clay), taking information on the three types of clay reported in the case study. Next, a weighted average was calculated for illite/smectite, kaolinite, and chlorite to define clay's elastic properties. Finally, reference values were set for the dominant minerals: quartz, potassium feldspars, and clay, as shown in Table 3.

For the construction of RPT in terms of  $\mu\rho$  and  $\lambda\rho$ , the heterogeneous isotropic method was applied for ternary plots. In

Figure 10, elastic properties of pure dominant minerals (quartz, potassium feldspar, and clay), denoted by diamonds, set the ternary RPT vertices for non-porous rock, i.e., the porosity of 0%. RPT bounds were calculated with the self-consistent method described above in Eqs. (1) to (3). In dashed lines, the sides of inner triangles represent 50% content of the dominant mineral portrayed in the opposite vertex. The ternary plots in black denote porosities of 0%, 15%, and 35%; intermediate plots in red are for 5% and 25%. In other words, the larger ternary plot

**Table 2.** Lithotypes related to rock's mineral composition. The classification used for 1D-3D lithotype interpretation on well logs and seismic inversion volumes. Feld: Feldspar, K: Potassium, and Qz: Quartz.

Lithology	Description
Shale	Clays > 50% > Quartz, K-Feldspar
Shaly Sandstone	Quartz, K-Feldspar ≤ 50% ≤ Clays
Feld K Sandstone	Quartz, Clays ≤ 50% ≤ K-Feldspar
Qz-Sandstone	Quartz > 50% > K-Feldspar, Clays

**Table 3.** Elastic properties of clays and the dominant rock minerals to build the specific ternary RPT for 1D-3D lithology interpretation.

Clays	Density (g/cm <sup>3</sup> )	Vp (km/s)	Vs (km/s)	Mineral	Density (g/cm <sup>3</sup> )	Vp	Vs
Illite/Smectite	2.40	3.6	1.85	Quartz	2.65	6.05	4.09
Kaolinite	1.58	1.44	0.93	K-Feldspar	2.62	4.68	2.39
Chlorite	2.60	4.90	3.23	Clay	2.47	2.77	1.21

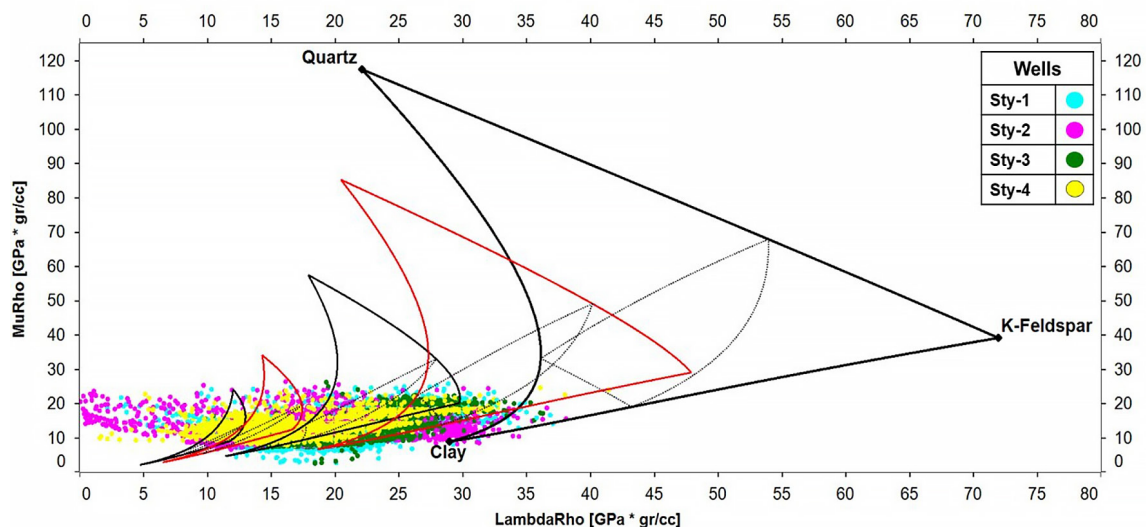


**Figure 10.** Construction of  $(\mu\rho - \lambda\rho)$  RPT with vertices defined by elastic properties of the calibrated dominant minerals, RPT bounds computed with micromechanics model. In color-filled points, elastic parameters of wells: Sty1, Sty2, Sty3, and Sty4.

in black is for 0% porosity, and the smaller is for 35%. Ternary plots decrease when porosity increases due to a lesser elastic contribution of pore-filling fluid.

In Figure 10, the elastic responses of wells from Figure 9 are plotted together with RPT. The point cloud of each color used corresponds to the elastic information of each of the four wells in the study area. Thus, the blue points correspond to Sty-1, green points to Sty-2, red points to Sty-3 well, and yellow points to Sty-4 well. The  $(\mu\rho - \lambda\rho)$  cross plot shows that well data and ternary RPT are in range. Some points often drop out of RPT bounds because they could involve more minerals than the dominant minerals considered; however, the framework of the proposed RPT-based interpretation is unaltered.

Once the characterization of the ternary RPT with elastic information of the four wells was achieved, Figure 11, the petroelastic interpretation of lithotypes was carried out. At this point, lithologies are defined by elastic responses of rock mixtures where the elastic contribution of pure minerals is considered. In Figure 11, the superimposed zones are mainly guided by the vertices of ternary plots. These are related to lithotypes described in Table 2 as follows: the yellow zone is trending to quartz vertex; therefore, quartz sandstone is straightforwardly discretized; the red zone is for the reservoir and is linked to sandstones, high porosities, and pore-filling fluid; green zone for shales is biased by clay vertex, grey zone is for k-feldspar sandstone, and the light green zone is for shaly sandstone.

Zones portrayed in Figure 11 are used to select points and differentiate between themselves. The filtered points are separately related to each lithotype for 1D petroelastic lithology interpretation. A third fundamental property, apart from  $\mu\rho$  and  $\lambda\rho$ , is the measured depth of elastic properties. Then lithotypes are

characterized in one-step along wells depth as shown in Figure 12. It is suggested that the characterization of lithotypes must be tied up with well geology reports. For instance, herein, Sty 1 reported massive intervals of k-feldspar sandstone and a better reservoir delineation. Modeling this information of correlated wells helped validate the novel petroelastic interpretation of lithology columns.

### 3.4. 3D petroelastic model for lithotype volume construction

1D petroelastic interpretation of lithologies is the main foundation for 3D petroelastic interpretation because the data design and visualization are analogous. In Figure 13, the validated ternary RPT was used in the same fashion as Figure 11. However, at this stage, the input data were calibrated volumes in terms of  $\mu\rho$  and  $\lambda\rho$ . They are cross-plotted, and RPT is superimposed to guide 3D lithology interpretation. In Figure 13, the colored zones are also related to the same lithotypes, i.e., green for shale, light green for shaly sandstone, grey for k-feldspar sandstone, yellow for quartz sandstone, and red for the reservoir.

The shaded zones were used to select and characterize volumes of seismic inversion data in  $\mu\rho$  and  $\lambda\rho$ . The result is a volume of lithotypes that quantifies each lithotype's position (x, y, z) and spatial distribution. 1D petroelastic interpretation from Figure 13 was used to tie up the lithotype volume obtained. Herein, in-line: 1,965 and x-line: 12,475 were used to show the main result of the proposed 3D petroelastic interpretation of lithologies. Figure 15 portrays the spatial distribution of shale, shaly sandstone, k-feldspar sandstone, quartz sandstone, and the reservoir. In addition, constructing sedimentary models and geobodies delineation could be its potential applications.

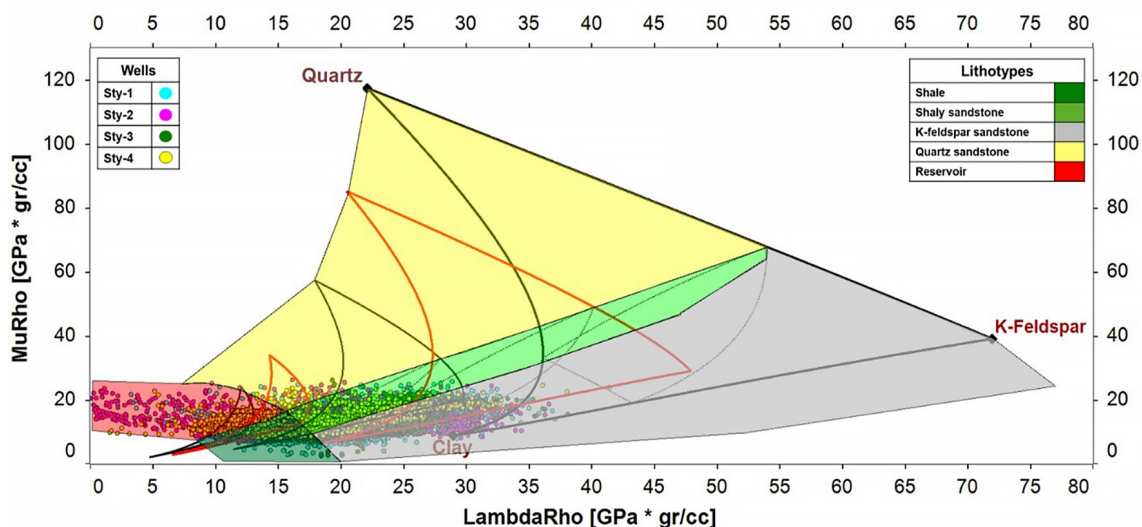


**Figure 11.** Ternary RPT shows the resulting lithotypes for the 1D model for the four wells, which would later be scaled to seismic to obtain a 3D geological model.

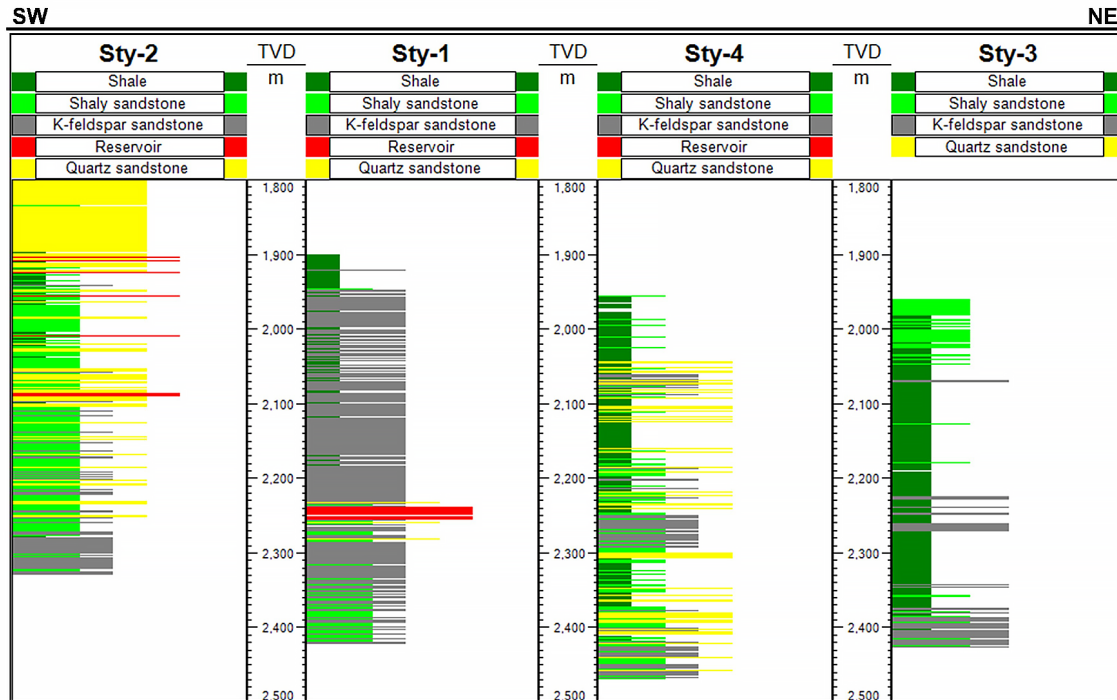


**Figure 12.** 1D petroelastic interpretation of lithologic columns. Cross-section correlation of lithology units colored with zones of Figure 11.

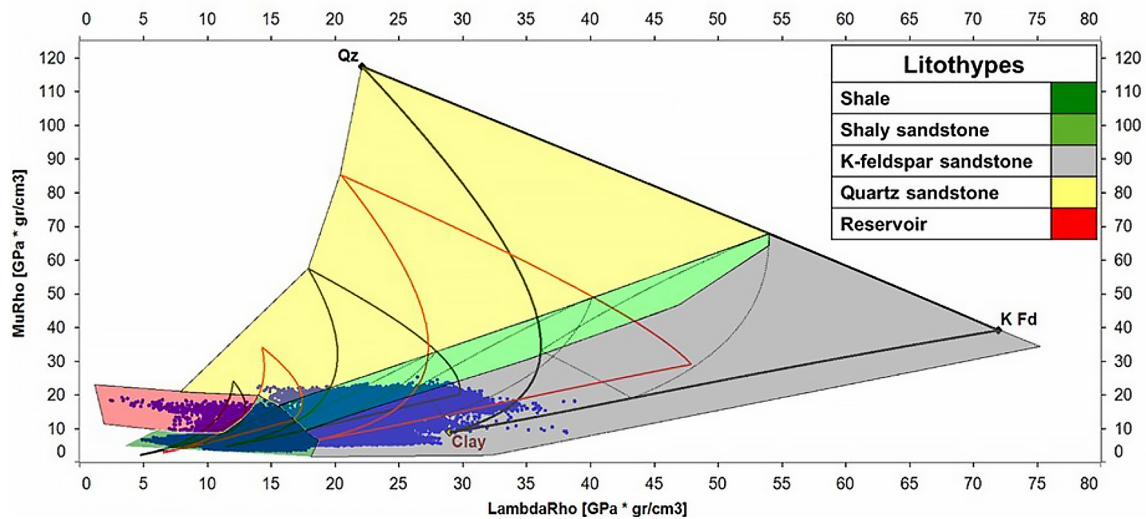


**Figure 13.** Shows the resulting lithotypes for the 1D model for the four wells, which would later be scaled to seismic to obtain a 3D geological model.

In Figure 15, stratal slice analysis focused on the spatial distribution of the reservoir was performed. Remember that this is a 3D visualization of the selection of intervals in red from Figure 13. These points are colored zones in red in Figures 14 and 15. Sty-1 well clearly dropped in the best zone of the reservoir because it landed in the broader area in red. Commercial

output is often linked to the vast presence of pore-filling fluid. In contrast, Sty-2 and Sty-3 were drilled in a sparse area in red. Sty-4, a re-entry of Sty-3, also dropped in a scarce area in red. The proposed 1D-3D interpretation of lithologies integrated with field and production well reports can assist in defining hydrocarbon-rich zones within the target stratum.

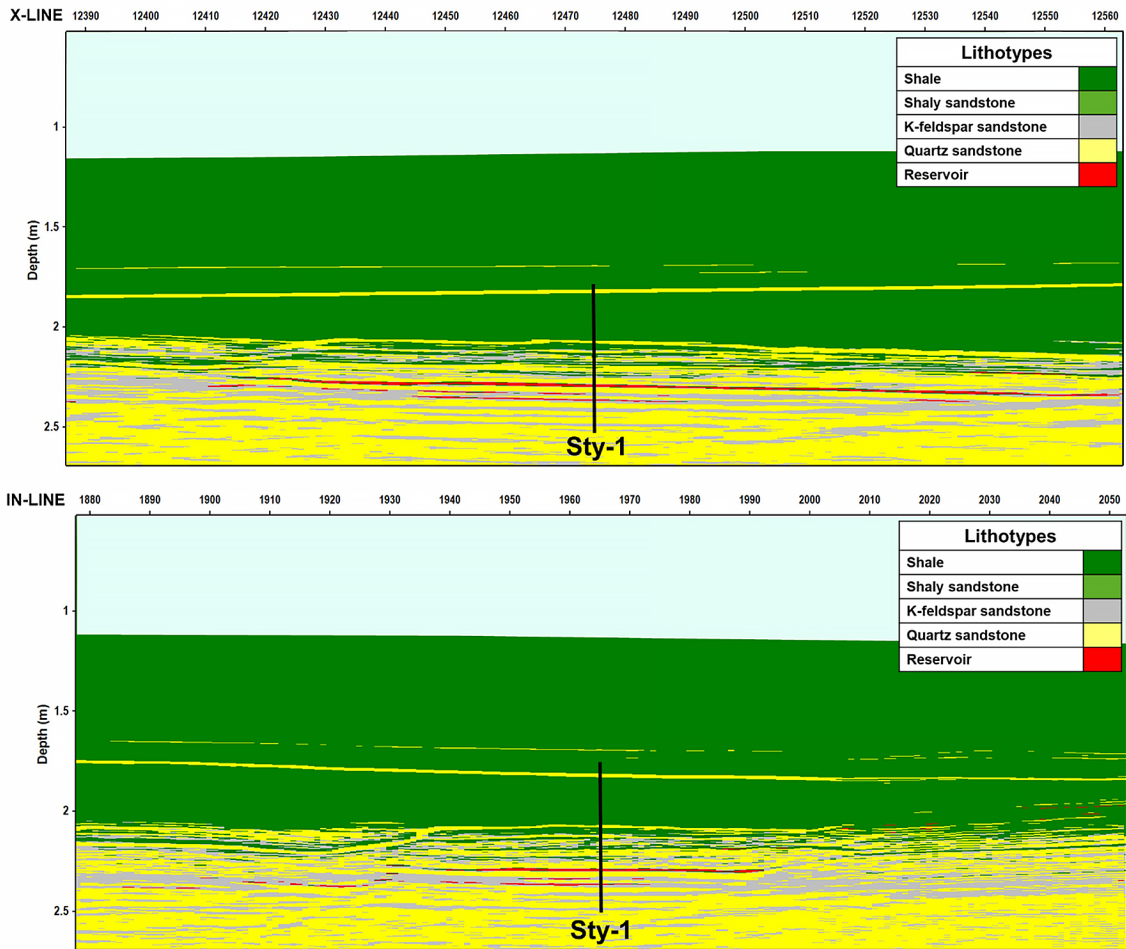


Figure 14. Lithotypes were obtained for the study case (In-line: 1,965; X-line: 12,475).

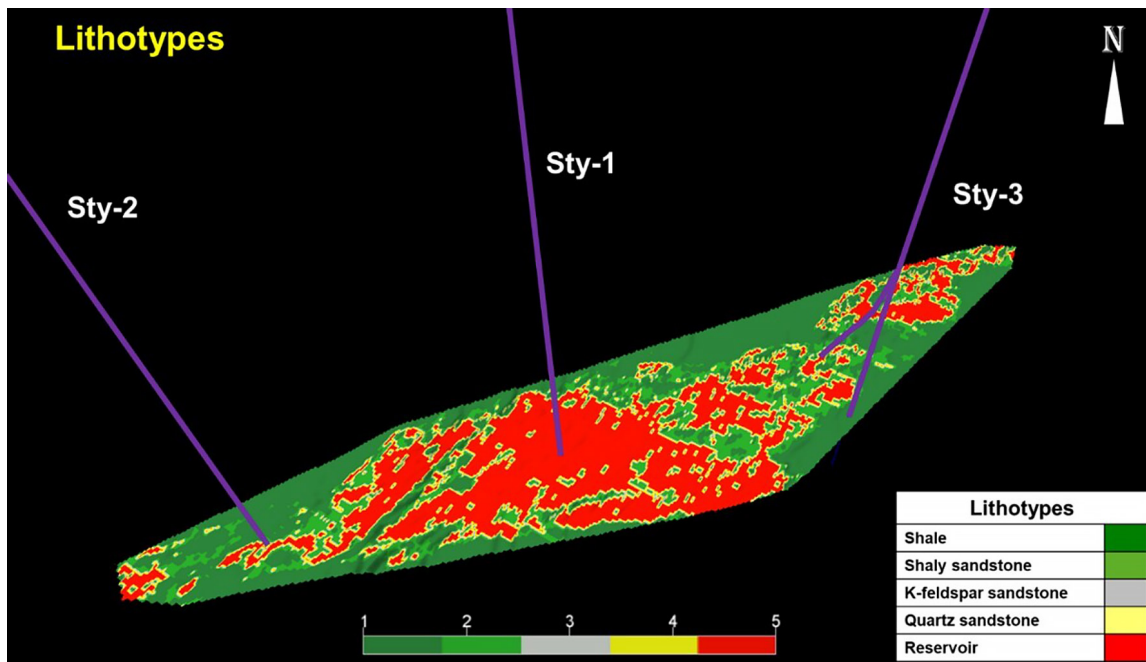


Figure 15. Stratal slice of reservoir identified by the rock physics templates RPT. The zone in red in Figure 13 encompasses the points distributed within the stratal slice.

### 3.5. 1D brittleness model

Integrating the petroelastic model of lithotypes and brittleness modeling is the major novelty of this research. Brittleness modeling reinforces 1D-3D petroelastic interpretation by quantifying brittleness in hydrocarbon-rich zones. Brittleness evaluation carried out based on Young's modulus  $E$  and Poisson's ratio  $\nu$  is well accepted in the oil industry, Section 2.2. Lab tests, well logs, and seismic inversion volumes can obtain these elastic parameters. Herein, the first step is to define the maximum and minimum values of  $E$  and  $\nu$ . In Table 5, the corresponding values are shown. They are related to dominant minerals with the highest and lowest values for  $E$  and  $\nu$ .

Next,  $E$  and  $\nu$  curves were calculated using geophysical logs modeled in section 3.1. The elastic parameters obtained for the wells are those presented in Figure 16.

With the elastic parameters defined and calculated for each well,  $E$  and  $\nu$  curves are normalized by applying equations 6 and 7. Brittleness indexes based on Young's modulus  $BI_E$  and Poisson's ratios  $BI_\nu$  are portrayed in Figure 17. They are qualitative indicators because they depend on the maximum and minimum values used. For instance, we used limits referenced in Table 4; however, the curve behavior will not change when other limits are used. The critical point is honoring the elastic properties of the most brittle and ductile formations.

Note that normalized profiles of  $BI_E$  are lesser than  $BI_\nu$  in

**Table 4.** Maximum and minimum values to  $E$  and  $\nu$  for brittleness analysis of the wells of the study case.

Parameter	Max	Min
E (GPa)	95.4	2.8
$\nu$ (Unitless)	0.44	0.07

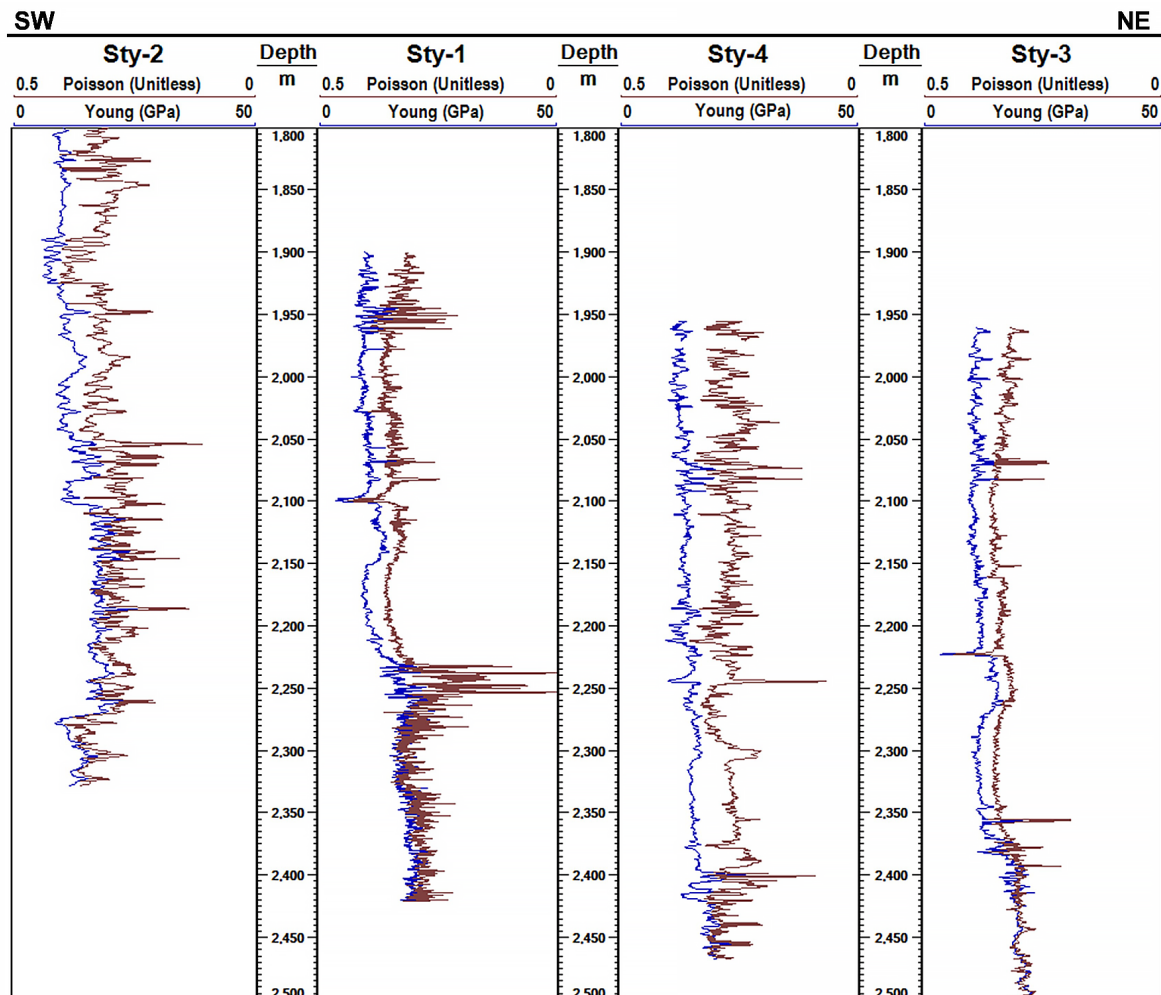


**Figure 16.** Elastic parameters  $E$  and  $\nu$  of the wells in the case study.

wells evaluated. This issue is because, in the discretization, the theoretical value of quartz with porosity equal to 0 was used as the maximum value for  $E$ . Therefore, we suggest using core data when available to maximum and minimum values for  $E$  and  $\nu$  at target formation. Finally, computing the arithmetic average of  $BI_E$  and  $BI_\nu$  with equation (8), the  $BA$  brittleness index was obtained and used to discriminate intervals with greater and lesser brittleness. Reservoir intervals reported are references to the brittleness quantification considering the elastic contribution of pore-filling fluid, Figure 18. Sty-1 reported a potent reservoir interval in contrast to Sty-3, which landed out of the hydrocarbon-rich zone. These well behaviors were linked to the performance of  $BA$  curves. Based on a qualitative interpretation of  $BA$  and the oil field data, the higher values ( $BA \gg 0.5$ ) could indicate the presence of hydrocarbons upon the target stratum.

It was obtained, and in the case of the Sty-1 well, the identification of the hydrocarbon zone. In Figure 18, the results of  $BA$  are shown.

### 3.6. 3D brittleness model

In the same fashion that was scaled 1D to 3D petroelastic interpretation of lithotypes, sections 3.3 and 3.4., 1D brittleness modeling was scaled to 3D brittleness modeling. Herein, 3D brittleness analysis was executed using volumes of Young's modulus and Poisson's ratio. These volumes came from seismic inversion tied with the area wells (Arévalo-López, 2017). Drawbacks about using data at different scales were solved in that step. For brevity, figures of intermediate normalizations of  $BI_E$  and  $BI_\nu$  were skipped. Results of 3D brittleness analysis based on  $BA$  are shown at the target stratum. Reservoir zones linked to  $BA$  were also investigated as an indicator of saturated zones. The latter represents an outstanding feature of lithotypes and brittleness workflows proposed.

Figure 19 shows 1D-3D brittleness modeling conducted on in-line and x-line corresponding to the intersection with the Sty-1. Zones in red denote higher values of the  $BA$  brittleness

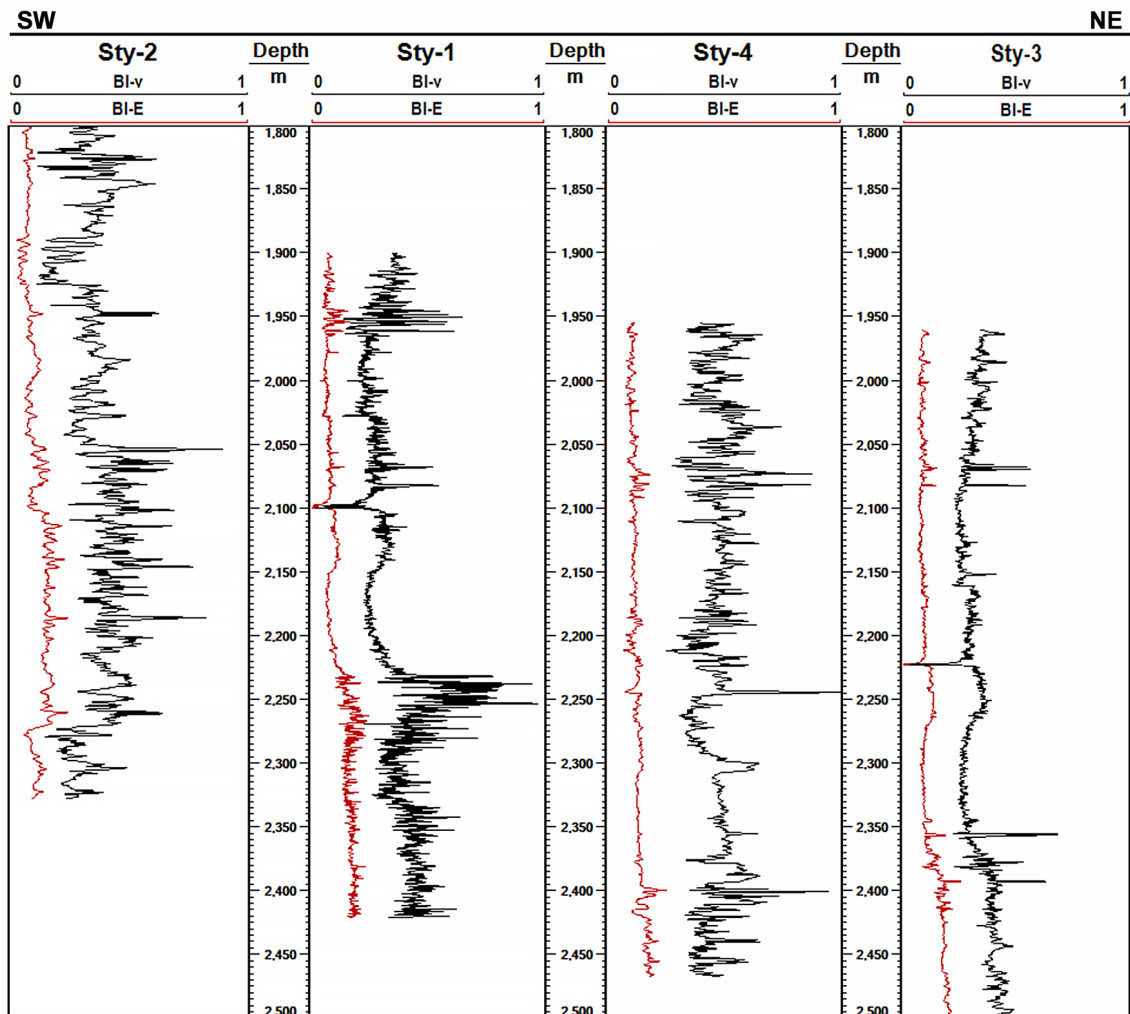
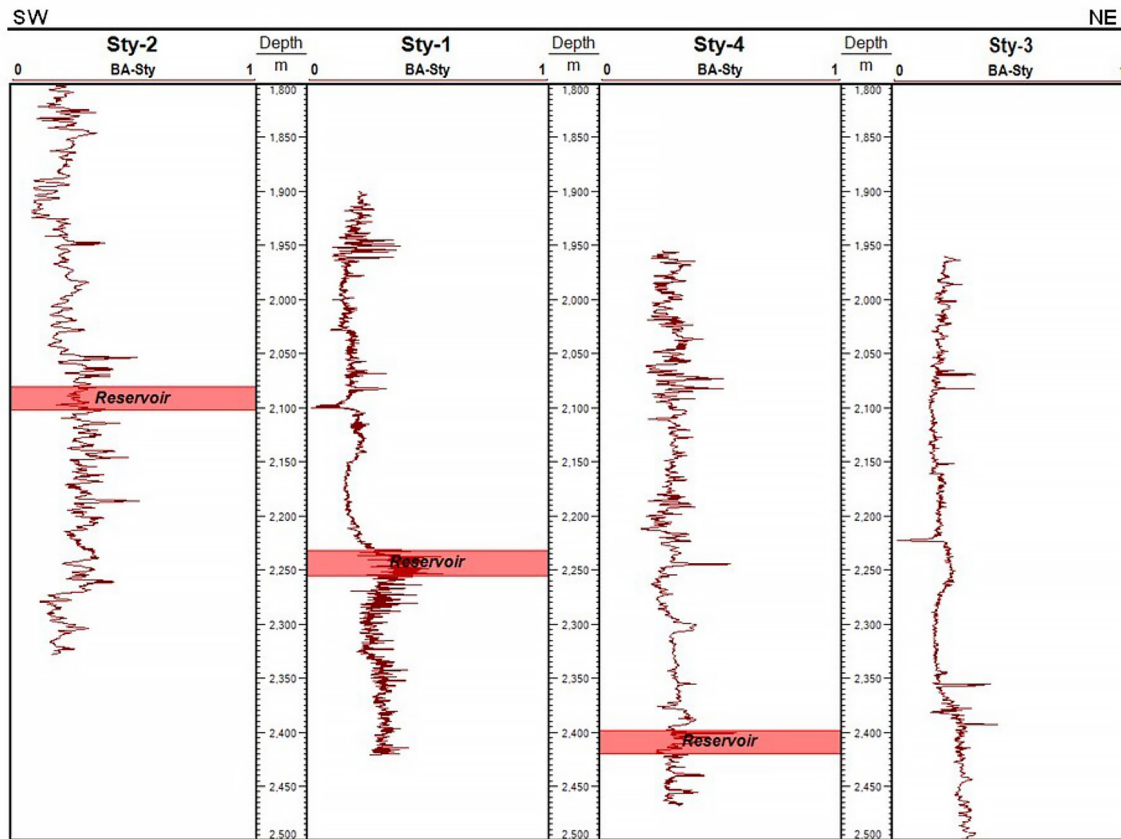


Figure 17. Brittleness indices,  $BI_E$  and  $BI_\nu$ , were calculated for wells of the case study.





**Figure 18.** Brittleness average (BA) based on a simple average of  $BI_E$  and  $BI_v$  to wells in the case study. Reservoir depths were used to calibrate the ranges of BA qualitatively.

index, consistent with the 1D brittleness analysis performed on Sty-1. The horizontal spatial distribution is related to the lateral continuity of brittle intervals at the target stratum, and vertical variations can underpin well paths to drill the most significant number of brittle intervals.

The same stratal slice, Figure 15, is used to portray the spatial distribution of brittle zones and landing area of the well paths, Figure 20. Regions in red were discriminated by cutting the higher values of the BA brittleness index. For example, at the target stratum, Sty-1 was placed into a sizeable brittle zone; Sty-2 and Sty-3 were drilled in poor brittleness zones; and Sty-4, a re-entry well from Sty-3, was redirected to an area with higher brittleness. This brittleness analysis carried out on wells and stratal slices, features the BA brittleness index as a new reservoir indicator.

Finally, in Figure 21, the integration of workflow results of both petroelastic interpretation and brittleness analysis are shown. The in-line: 1965 and cross-line: 12765 corresponds to Sty-1, and the reservoir zone in red was identified at well scale and delineated at seismic scale. 3D visualization of lithotype distribution, Figure 15, and higher values of BA ( $\gg 0.5$ ), Figure 20, are merely depicted and correlated with Sty-1.

#### 4. Discussion

Following the proposed methodology (Section 2, Figure 4), it was possible to determine, with the support of the  $\mu\rho-\lambda\rho$  RPT the petroelastic facies and confirm the reservoir zone at 1D (Figure 12) and 3D (Figures 14 and 15). However, particularly for the Sty-1 well, a better correlation of parameters and identification of the reservoir area was obtained concerning the other wells evaluated. It may be because available information was calibrated with this well. Additionally, with the Brittleness methodology (Section 2, Figure 5), results were also found at well level 1D (Figure 19) and 3D seismic (Figures 19 and 20) scale, consistent with what was described in the literature and what was obtained with the petroelastic method described in the previous paragraph. Particularly for this case, the brittle and ductile zones were distinguished employing the BA parameter (Figures 19, 20, and 21), observing that for the former ( $BA \gg 0.5$ ), the attenuation caused by the presence of hydrocarbons allows the identification of the reservoir, due to the nature of the method that does not involve the bias of the user. Here, the 1D brittleness evaluation (Lizcano-Hernández *et al.*, 2018) was clearly extended to 3D

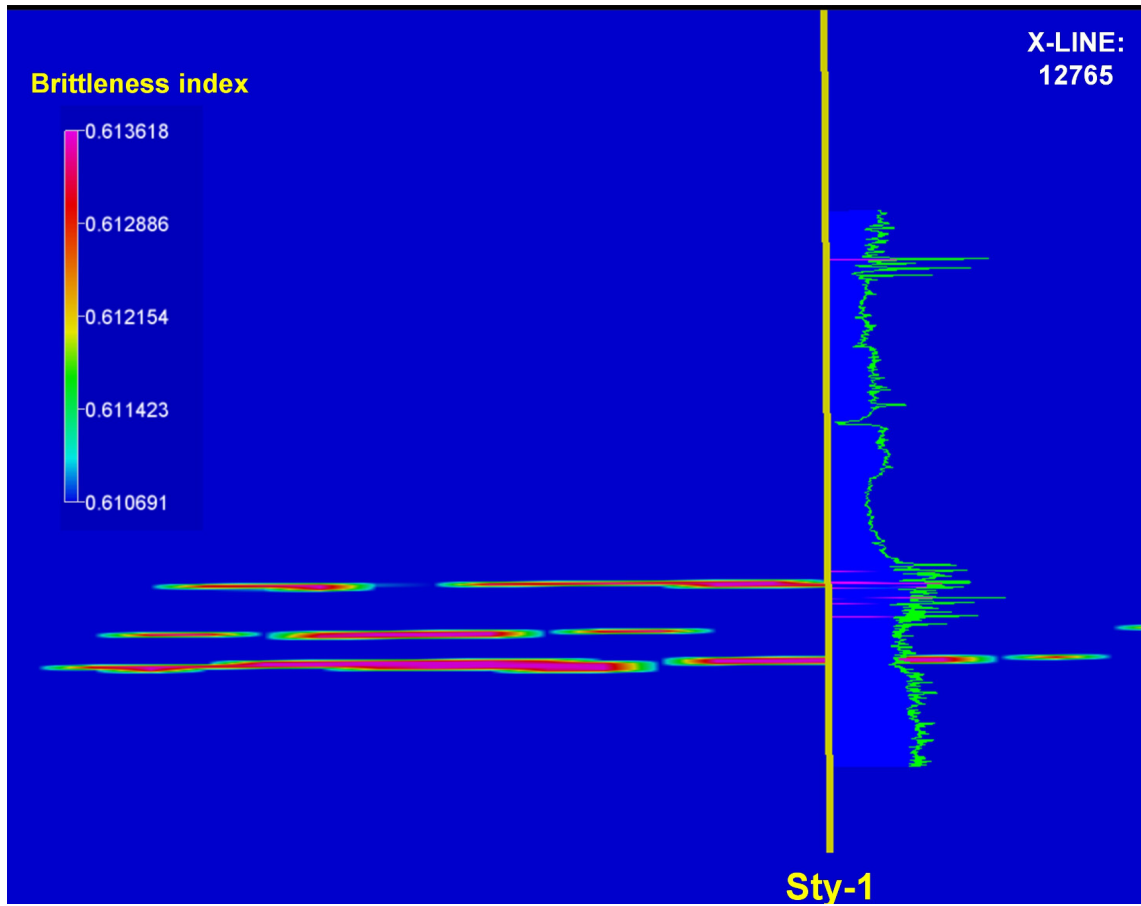


Figure 19. Brittle zones in red from 1D-3D brittleness analysis of the case study. Sty-1 is used as a correlation well.

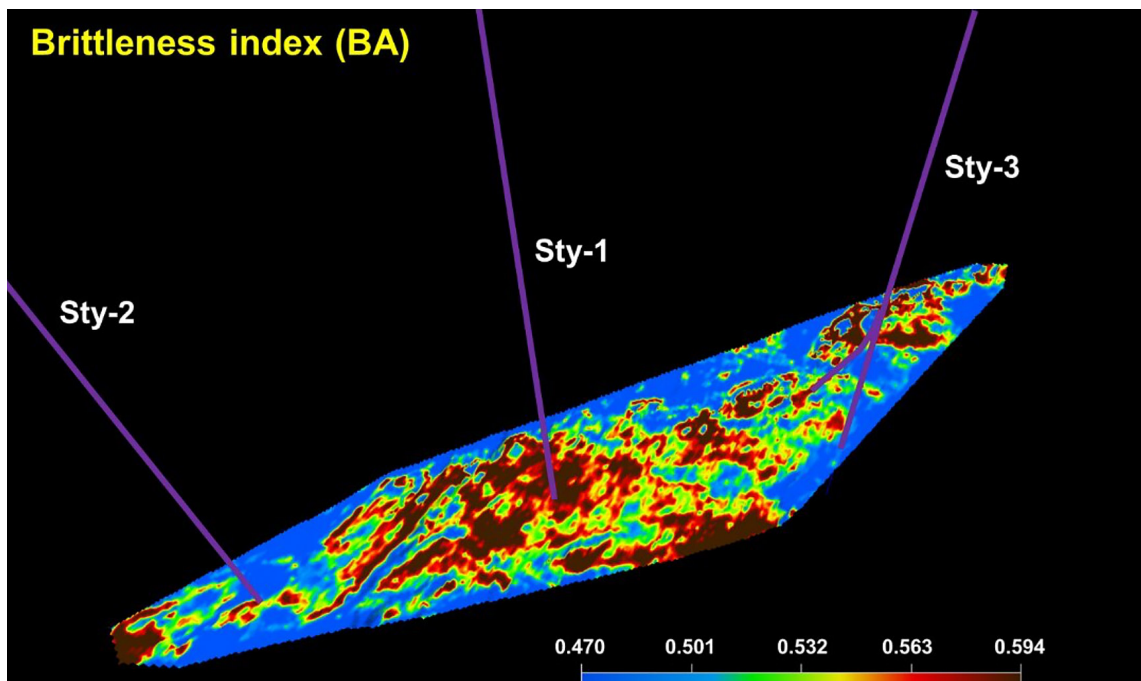
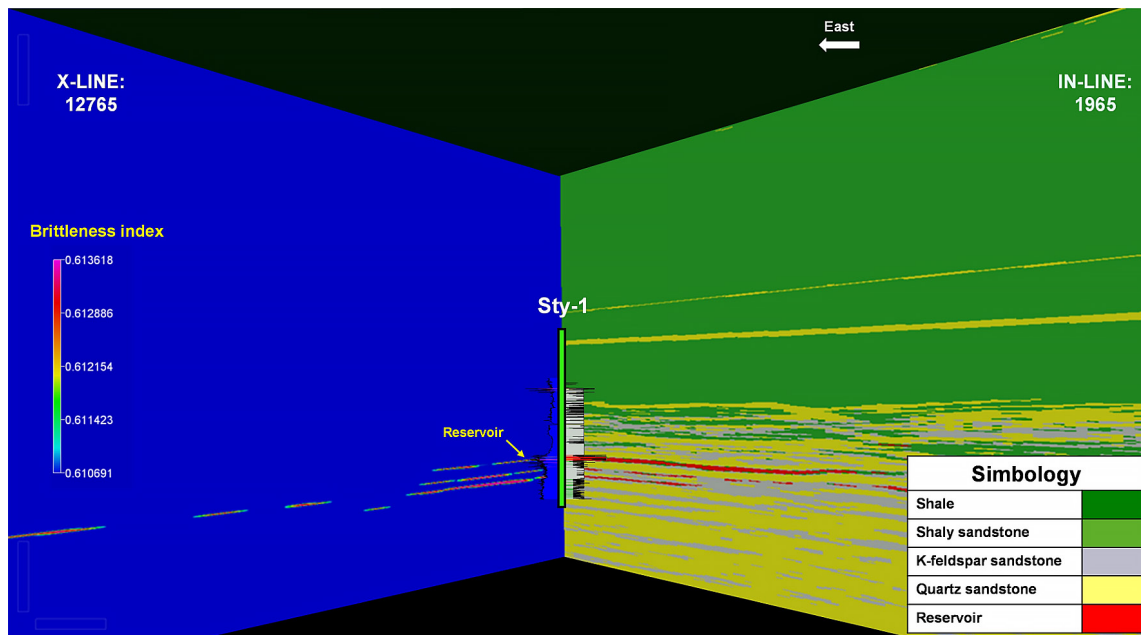


Figure 20. Reservoir identification using the brittleness index modeling. BA index was set out as a reservoir indicator in terrigenous formations.



**Figure 21.** Results coupled of the brittleness analysis and lithology interpretation of the study case.

brittleness analysis to identify zones of potential reservoirs. This quantitative method of  $E - v$  brittleness analysis enables us to identify the hydrocarbon zones sufficiently and reinforce the determinations of the conventional qualitative methods solely based on geology principles.

## 5. Conclusions

The results obtained from the lithotypes, at the well level and the seismic level, permit the identification of the reservoir zones, which were concordant at both levels of analysis. The effectiveness of the petroelastic workflow proposed as a complement to calibrate conventional exploratory analyzes was ascertained. The proposed methodology supported in the RPTs established the identification of lithologies at the log level, consistent with published results, which assisted defining and scaling the lithologies to the seismic one, with volumes of valuable subsurface information obtained.

Applying the proposed methodology, it was possible to determine the spatial distribution of the reservoir, which honors the results obtained independently for each of the wells, as well as confirm what has been reported in the literature for the study area. In the same way, the methodology allowed identifying the zones in which, according to what was reported, there are no reservoir conditions, as is the case of the Sty-3 well. It has also been possible to contribute to the quantitative seismic interpretation from the results obtained from the brittleness modeling both at

the well and seismic levels. With the above, it is noted that this method has great potential since it is through calculations and not the interpreter's subjectivity that the zones of the potential reservoir were differentiated.

In the lithological interpretation carried out with the RPT, the areas with hydrocarbon content that allowed their identification were attenuated. Additionally, the workflow for brittleness analysis was applied at the well and seismic level, which confirmed the areas of the reservoir with the best conditions for the prospective location of wells. While in the quantitative estimation carried out with the brittleness modeling, it was determined that the reservoir zones are found in  $BA$  brittleness index greater than 0.5. Also, in the application of the said methodology, it is the  $BI_v$  brittleness obtained for Poisson's ratio, which is the most sensitive to attenuation due to hydrocarbon content, for which it is proposed to carry out tests in which  $BA$  is obtained, through averages of a different nature than arithmetic to refine the areas of potential reservoir more.

## Acknowledgments

Authors are thankful to Instituto Mexicano del Petróleo for supporting this research. They are also grateful the valuable suggestions from peer reviewers to improve the article's quality. DLA and MADC thank to CONAHCYT for the graduated scholarship granted. Stanford University provided the seismic

information used in this work and consists of the and volumes produced from a simultaneous impedance inversion process.

## References

- Anatoly S. (1999). Mathematical models of elastic wave processes in seismology and seismic prospecting: forward and inverse problems. *Simulation Practice and Theory*, 7, 125-151. Computing Center, Siberian Division, Russian Academy of Sciences, November 1998.
- Arévalo-López, H. S., (2017). Petro-Elastic Interpretation of Seismic Impedances. Dissertation for the Degree of Doctor of Philosophy at Stanford University, June 2017. <http://purl.stanford.edu/yb330pn2762>.
- Areválo-López, H. S. and Dvorkin, J. P., (2017). Simultaneous impedance inversion and interpretation for an offshore turbiditic reservoir, *Interpretation*, 5(3), SL9-SL23, doi: <https://doi.org/10.1190/INT-2016-0192.1>
- Avseth, P., Mukerji, T., and Mavko, G. (2005). Quantitative Seismic Interpretation. Applying Rock Physics to Reduce Interpretation Risk. Cambridge, New York, Melbourne: Cambridge University, doi: <https://doi.org/10.1017/S0016756806233053>
- Bredesen, K., Lorentzen, M., Nielsen, L., and Mosegaard, K. (2021). Quantitative seismic interpretation of the Lower Cretaceous reservoirs in the Valdemar Field, Danish North Sea. Department of Geophysics, Geological Survey of Denmark and Greenland (GEUS), Copenhagen, Denmark (July 2021). doi: <https://doi.org/10.1144/petgeo2021-016>
- Byoung, Y.K. (2016). Prestack elastic generalized-screen migration for multicomponent data. *Journal of Applied Geophysics*, 126, 116–127, doi: <https://doi.org/10.1016/j.jappgeo.2016.01.016>
- Chengbo, Y. (2016). Effects of porosity on seismic velocities, elastic moduli and Poisson's ratios of solid materials and rocks. *Journal of Rock Mechanics and Geotechnical Engineering* 8. doi: <https://doi.org/10.1016/j.jrmge.2015.07.004>
- Carcione, J., and Avseth, P. (2015). Rock-physics templates for clay-rich source rocks. *Geophysics*, 80, D481-D500. doi: <https://doi.org/10.1190/geo2014-0510.1>
- Danaei, S., Silva-Neto, G.M., Schiozer, D.J., and Davolio A. (2020). Using the petro-elastic proxy model to integrate 4D seismic in ensemble-based data assimilation. *Journal of Petroleum Science and Engineering*, 194, 107457. doi: <https://doi.org/10.1016/j.petrol.2020.107457>
- Ementon, N., Hill, R., Flynn, M., Motta, B., and Sinclair, S. (2004). Stybarrow Oil Field—From Seismic to Production, the Integrated Story so Far. Society of Petroleum Engineers (SPE 88574), Perth, Australia, October 2004. doi: <https://doi.org/10.2118/88574-MS>
- Gavin, L. J. (2015). Stress-induced seismic azimuthal anisotropy offshore NW Australia. Doctoral Thesis, The University of Western Australia. <https://research-repository.uwa.edu.au>
- Goodway, B., Perez, M., Varsek, J., and Abaco, C. (2010). Seismic petrophysics and isotropic-anisotropic AVO methods for unconventional gas exploration. *The Leading Edge*, 29(12), 1500-1508. doi: <https://doi.org/10.1190/1.3525367>
- Holt, R., and Westwood, B. (2016). Predicting mineralogy from elastic rock properties. *CSEG RECORDER*, 41, 22-26. <https://csegrecorder.com/articles/view/predicting-mineralogy-from-elastic-rock-properties>
- Lizcano-Hernández, E. G., Nicolás-López, R., Valdiviezo-Mijangos, O. C. and Meléndez-Martínez, J. (2018). Estimation of brittleness indices for pay zone determination in a shale-gas reservoir by using elastic properties obtained from micromechanics. *Journal of Geophysics Engineering* 15, 307–314, doi: <https://doi.org/10.1088/1742-2140/aa9a5e>
- López-Aguirre, D., García-Benitez, S. R., and Nicolás-López, R. (2020). Obtención de la velocidad de corte y parámetros elásticos-geomecánicos, utilizando redes neuronales. *AIPM Petroleum Engineering Journal*, 60(2), ISSN 0185-3899. <https://aipmac.org.mx/editorial/revista-ingenieria-petrolera/ediciones-2020>
- Mardani, R. A. (2020). Generating Synthetic Seismogram in Python, Online Short Course, EAGE, October 2020.
- Nicolás-Lopez, R., and Valdiviezo-Mijangos, O. C. (2016). Rock physics templates for integrated analysis of shales considering their mineralogy, organic matter and pore fluids. *Journal of Petroleum Science and Engineering*, 137, 33-41. doi: <https://doi.org/10.1016/j.petrol.2015.11.009>
- Uhlemann, S., Hagedorn, S., Dashwood, B., Maurer, H., Gunn, D., Dijkstra, T., and Chambers, J. (2016). Landslide characterization using P- and S-wave seismic refraction tomography — The importance of elastic moduli. *Journal of Applied Geophysics*, 134, 64–76. doi: <https://doi.org/10.1016/j.jappgeo.2016.08.014>
- Valdiviezo-Mijangos, O. C., and Nicolás-López, R. (2014). Dynamic characterization of shale systems by dispersion and attenuation of P- and S-waves considering their mineral composition and rock maturity. *Journal of Petroleum Science and Engineering*, 122, 420-427. doi: <https://doi.org/10.1016/j.petrol.2014.07.041>
- Zhiheng, J. (2019). Seismic inversion for fluid bulk modulus based on elastic impedance. *Journal of Applied Geophysics*, 169, 74-84. doi: <https://doi.org/10.1016/j.jappgeo.2019.06.013>
- Zoback, M. D. (2007). Reservoir Geomechanics. Department of Geophysics, Stanford University. Cambridge University Press. The Edinburgh Building, Cambridge CB2 8RU, UK. doi: <https://doi.org/10.1190/geo2018-0700.1>